

This is the accepted manuscript made available via CHORUS. The article has been published as:

Landauer, Kubo, and microcanonical approaches to quantum transport and noise: A comparison and implications for cold-atom dynamics

Chih-Chun Chien, Massimiliano Di Ventra, and Michael Zwolak

Phys. Rev. A **90**, 023624 — Published 18 August 2014

DOI: [10.1103/PhysRevA.90.023624](https://doi.org/10.1103/PhysRevA.90.023624)

Landauer, Kubo, and microcanonical approaches to quantum transport and noise: A comparison and implications for cold-atom dynamics

Chih-Chun Chien¹, Massimiliano Di Ventra², and Michael Zwolak³

¹*School of Natural Sciences, University of California, Merced, CA 95343, USA*

²*Department of Physics, University of California, San Diego, CA 92093, USA*

³*Department of Physics, Oregon State University, Corvallis, OR 97331, USA*

We compare the Landauer, Kubo, and microcanonical [J. Phys. Cond. Matter **16**, 8025 (2004)] approaches to quantum transport for the average current, the entanglement entropy and the semiclassical full-counting statistics (FCS). Our focus is on the applicability of these approaches to isolated quantum systems such as ultra-cold atoms in engineered optical potentials. For two lattices connected by a junction, we find that the current and particle number fluctuations from the microcanonical approach compare well with the values predicted by the Landauer formalism and FCS assuming a binomial distribution. However, we demonstrate that well-defined reservoirs (i.e., particles in Fermi-Dirac distributions) are not present for a substantial duration of the quasi-steady state. Thus, on the one hand, the Landauer assumption of reservoirs and/or inelastic effects is not necessary for establishing a quasi-steady state. Maintaining such a state indefinitely requires an infinite system, and in this limit well-defined Fermi-Dirac distributions can occur. On the other hand, as we show, the existence of a finite speed of particle propagation preserves the quasi-steady state irrespective of the existence of well-defined reservoirs. This indicates that global observables in finite systems may be substantially different from those predicted by an uncritical application of the Landauer formalism, with its underlying thermodynamic limit. Therefore, the microcanonical formalism which is designed for closed, finite-size quantum systems seems more suitable for studying particle dynamics in ultra-cold atoms. Our results highlight both the connection and differences with more traditional approaches to calculating transport properties in condensed matter systems, and will help guide the way to their simulations in cold-atom systems.

PACS numbers: 72.10.Bg, 67.10.Jn, 05.60.Gg

I. INTRODUCTION

Experimental investigations of transport phenomena in ultra-cold atoms confined in engineered optical potentials offer a test bed for transport theories at the nanoscale. Several phenomena, such as the sloshing motion of an atomic cloud in optical lattices [1], directed transport using a quantum ratchet [2], relaxation of noninteracting and interacting fermions in optical lattices [3], and others have been demonstrated. Their applications in atomtronics [4], which aims at simulating electronics by using controllable atomic systems, are promising [5–9]. It is thus important to develop proper theoretical and computational methods to direct future progress in this field.

Due to the quantum nature of atoms, finite particle numbers, and small sizes of these systems, the applicability of semi-classical approaches, such as the Boltzmann equation, become questionable. The Landauer formalism [10, 11], which has been widely implemented in mesoscopic physics, is naturally appealing for studying transport phenomena in ultra-cold atoms. Those approaches and their generalizations have been applied to study various problems in cold atoms [12–17]. In addition to steady-state properties, one may want to study fluctuation effects and correlations using full-counting statistics (FCS) [18]. An examination of the underlying assumptions of those well-known formalisms, however, raise questions on their applicability to ultra-cold atoms.

The Landauer formalism, which is designed for open systems, assumes the existence of two reservoirs that supply particles to be transmitted through a junction region. Since the particle number and energy (when no external time-dependent

fields are present) in ultra-cold atomic experiments are (to a very good approximation) conserved, the concept of a reservoir does not necessarily hold. FCS generally assumes the transmitted particles behave like billiards with a well-defined tunneling probability distribution. Whether such an assumption holds true in finite, closed systems will determine whether the formalism can be applied to cold atom experiments as well.

An alternative approach for studying transport in quantum systems is within the *microcanonical formalism* (MCF) [11, 19, 20]. This formalism is based on using closed quantum systems driven out of equilibrium by a change of parameters (e.g., an external bias or a density imbalance) to calculate transport properties. The conservation of particle number and energy are naturally built into this formalism, and there is no need to introduce reservoirs and one can fully preserve the wave nature of the particles. This formalism has also been integrated with density-functional theory for investigating quantum transport through atomic or molecular junctions [21, 22]. The microcanonical formalism is particularly suitable for ultra-cold atoms, which are accurately modeled as isolated quantum systems. In this respect, the formalism has already been developed to study transport phenomena in these systems [23–28].

The goal of this paper is to compare the microcanonical approach to the Landauer formalism and determine which assumptions lead to the same observables, such as the average current and FCS. The MCF is generically applicable to closed quantum systems, and here we use transport of ultra-cold non-interacting fermions in one-dimensional (1D) optical lattices

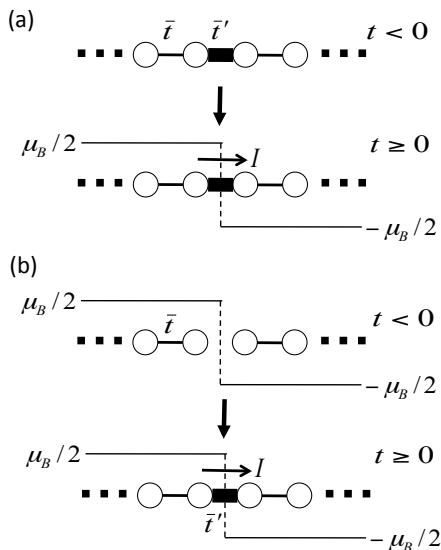


Figure 1. Schematic of a one dimensional lattice and transport induced by (a) application of a bias at $t = 0$, where a step-function bias is applied to the system and a current flows through the middle link or (b) connecting a link between the two initially disconnected parts at $t = 0$.

as a particular example. A possible setup is shown in Figure 1. Unlike electronic systems where the Coulomb interactions cannot be really switched off, and therefore for which this comparison would be more academic, cold atoms experiments allow for a relatively easy tuning of interactions among particles down to the non-interacting limit. The microcanonical formalism can, of course, be applied to systems with Coulomb interactions. However, here we focus only on its applications to noninteracting cold-atom systems. While electrons are naturally confined in solid-state systems, a background harmonic trapping potential is often implemented in addition to the optical lattice for confining atoms. However, recent advance in trapping atoms in ring-shape geometries [5, 29] or a uniform potential [30] makes it possible to consider homogeneous cold-atom systems. Moreover, a weak background harmonic potential does not change the qualitative conclusions from the MCF, as illustrated in Ref. [23]. Therefore we focus here on the dynamics of cold atoms in optical lattices without a background harmonic trapping potential.

We find that the steady-state current and particle number fluctuations from the microcanonical formalism approach the values of the average current and FCS predicted from the Landauer formalism already at moderate system sizes. However, we also find – for finite times – that one of the assumptions of the Landauer formalism is unnecessary: The particle distributions in the two lattices supplying/absorbing particles do not need to be populated according to Fermi-Dirac distributions. In fact, their occupation deviates from the equilibrium distribution during the whole duration of a quasi-steady state. Furthermore, the results from the microcanonical formalism agree with the predictions from the FCS semi-classical formula by assuming a binomial distribution of the transmitted

particles, ruling out alternative semi-classical descriptions. To connect the different approaches, we also develop a Kubo formalism based on the microcanonical picture of transport, which we use to calculate explicit expressions for transport in closed systems. This gives us an analytical method to investigate dynamical transport phenomena in nanoscale and ultra-cold atomic systems.

In addition to the average current and FCS, we also investigate the dynamical evolution of the entanglement entropy, which quantifies the correlations between two connected systems. The entanglement entropy is of broad interest in many fields, ranging from black hole physics [31] to quantum information science [32]. This quantity can be easily evaluated using the microcanonical formalism. A semi-classical formula based on FCS of two noninteracting fermionic systems connected by a junction has been derived in Ref. [18] and generalized to many-body systems [33, 34]. Ref. [18] predicts a linear growth of the entanglement entropy as time increases. Again, we find that the results from the microcanonical formalism match the prediction from the semi-classical formula by assuming a binomial distribution of the transmitted particles. Assuming an alternative distribution results in predictions that are readily distinguishable.

This paper is organized as follows: Section II reviews the Landauer formalism and its assumptions. Section III introduces the microcanonical formalism and its applications. The spatially resolved current from the MCF is discussed in Section IV. Section V reviews the FCS. Section VI shows the absence of memory effects in transport of noninteracting fermions. Section VII compares the results from the MCF and Landauer formalism. Importantly, the deviation from the equilibrium Fermi-Dirac distribution is clearly demonstrated. Section VIII shows the light-cone structure of wave propagation monitored by the MCF. Section IX reviews the Kubo formalism and how it helps connect the two approaches. Finally, Section X concludes our study with suggestions of future work.

II. LANDAUER FORMALISM

By assuming the existence of a steady-state current between two reservoirs bridged by a central link, the current can be estimated from the Landauer formula with the help of, e.g., Green's functions [10, 11]. For a detailed description of the physical assumptions behind this formalism we refer the reader to Ref. [11]. Here, we mention only the assumptions that will be relevant for our comparison with the microcanonical formalism: (1) A steady-state current is *assumed* to exist. Whether a steady-state current always emerges from a given nonequilibrium condition is not at all obvious [11]. (2) Two macroscopic reservoirs – holding noninteracting fermions populated according to Fermi-Dirac distributions – are also assumed. The separation of the system into reservoirs and a region of interest is not always easy to determine for an actual physical structure. (3) The transport at the junction does not provide any feedback to the reservoirs.

While one can construct configurations where a steady-

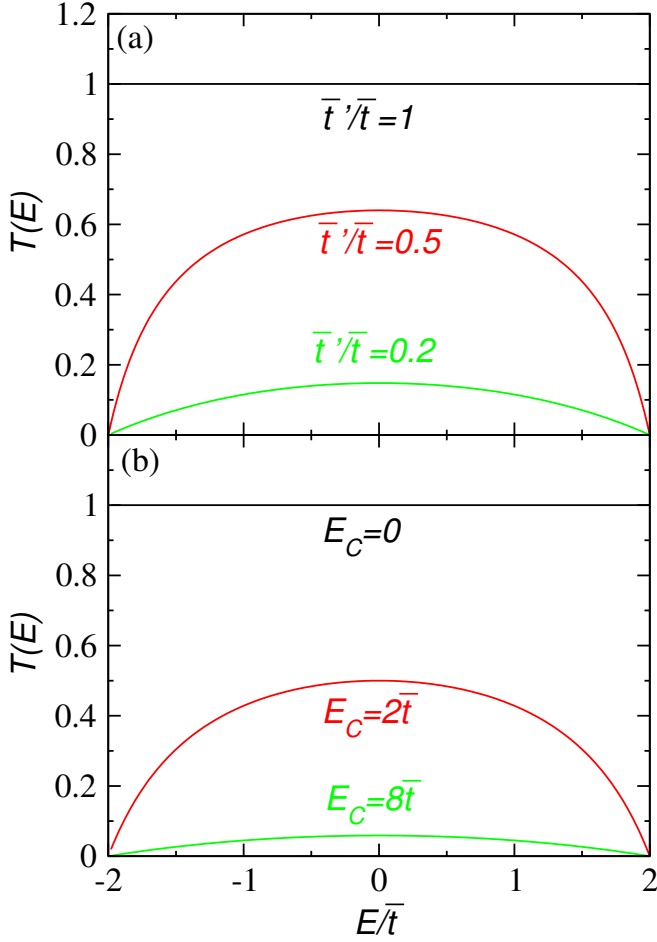


Figure 2. (Color online) The transmission coefficients $T(E)$ at $\mu_B = 0$ for (a) the weak-link case ($\bar{t}'/\bar{t} = 1, 0.5, 0.2$ from top to bottom) and (b) the central-site case ($E_C/\bar{t} = 0, 2, 8$ from top to bottom).

state current does not exist [35], in the case where two 1-D chains are connected by a central junction (as considered in this paper), there is always a steady-state current, as will be verified in the microcanonical formalism (see Section IV). Therefore, we do not focus here on assumption (1), but rather on (2) and (3). As will be shown in Sec. VII, the distributions on both sides deviates from the Fermi-Dirac distribution when the system maintains a steady state so assumption (2) is not necessary for observing a steady-state current. Moreover, Section VIII will show that density changes can propagate into regimes away from the junction so there can be feedback and assumption (3) is also not necessary.

On the other hand, in this section we calculate the current using the Landauer formalism for two configurations of a junction between two 1D lattices. One can insert a link with a tunable hopping coefficient \bar{t}' in the middle of a chain, which we call the *weak-link case*, or insert a central site with tunable on-site energy E_C , which we call the *central-site case*. In cold-atom experiments it has been shown that one can suppress the transmission of atoms by introducing an optical barrier [5] or by introducing a constriction in the trapping potential [6]. Therefore the tunneling coefficient and onsite energy

may be tuned simultaneously. Here we separate the effects of tuning the two parameters and one will see that there is no observable difference if the transmission coefficient T can be found and physical quantities are compared at the same T . We consider a uniform bias $E_L = \mu_B/2$ on the left half and, similarly, $E_R = -\mu_B/2$ on the right half. By making the two lattices on both sides semi-infinite, they behave as the two reservoirs with different electrochemical potentials. The hopping coefficient is denoted by \bar{t} and the unit of time is $t_0 = \hbar/\bar{t}$. We set the electric charge $e \equiv 1$ and $\hbar \equiv 1$. The length is measured in units of the lattice constant.

The Green's function of the left (right) semi-infinite chain can be derived using recursive relations, which lead to [36] $G_{L(R)}(E) = 1/[E - E_{L(R)} - \Sigma_{L(R)}(E)]$, where $\Sigma_{L(R)} = (1/2)[E - E_{L(R)} - i\sqrt{4\bar{t}^2 - (E - E_{L(R)})^2}]$. The retarded Green's function of the junction is $G(E) = 1/[E - E_C - \Sigma_{CL} - \Sigma_{CR}]$, where $\Sigma_{CL(CR)} = V_{CL(CR)}^2 G_{L(R)}(E)$ and $V_{CL(CR)}$ is the coupling to the left (right) chain [11, 37]. The current (including both spins) is [11]

$$I = \frac{1}{\pi} \int_{-\infty}^{\infty} dE (f_L - f_R) T(E) = \frac{1}{\pi} \int_{-\mu_B/2}^{\mu_B/2} dE T(E), \quad (1)$$

where the reservoirs are taken to be at zero temperature, as we will throughout this work. The transmission coefficient is

$$T(E) = \Gamma_L \Gamma_R |G(E)|^2, \quad (2)$$

where $f_{L(R)}$ denotes the density distribution of the left (right) chain, i.e., the Fermi-Dirac distribution function, and $\Gamma_{L(R)} = -2\text{Im}\Sigma_{CL(CR)}$.

For a uniform chain with $\bar{t}' = \bar{t}$, $V_{CL(CR)} = \bar{t}$. After some algebra, the current is given by

$$I = \frac{1}{\pi} \int_{-\mu_B/2}^{\mu_B/2} \frac{4g_L g_R dE}{\mu_B^2 + (g_L + g_R)^2}, \quad (3)$$

where $g_{L(R)} = \sqrt{4\bar{t}^2 - (E - E_{L(R)})^2}$. To the leading order of μ_B , Eq. (3) gives $I \simeq \mu_B \bar{t}/\pi$. Moreover, it can be shown that $T(E=0) \rightarrow 1$ as $\mu_B \rightarrow 0$.

For the weak-link case, if we take the last site of the left chain as the central site, $V_{CL} = \bar{t}$, $V_{CR} = \bar{t}'$, and $E_C = E_L$. The current is

$$I = \frac{1}{\pi} \int_{-\mu_B/2}^{\mu_B/2} \frac{4g^2 g_L g_R dE}{[(E - E_L) - g^2(E - E_R)]^2 + (g_L + g^2 g_R)^2}, \quad (4)$$

where $g \equiv (\bar{t}'/\bar{t})$. When $g \ll 1$, to the leading order of g and then to the leading order of μ_B , one obtains $I \simeq 4\mu_B g^2 \bar{t}/\pi$. For the central-site case, $V_{CL} = V_{CR} = \bar{t}$ and E_C can be tuned. The current is

$$I = \frac{1}{\pi} \int_{-\mu_B/2}^{\mu_B/2} \frac{4g_L g_R dE}{(E_L + E_R - 2E_C)^2 + (g_L + g_R)^2}. \quad (5)$$

Figure 2 shows $T(E)$, which is symmetric about $E = 0$, for both cases with selected parameters.

III. MICRO-CANONICAL FORMALISM

In the micro-canonical approach to quantum transport [19], one considers a finite system (say two electrodes and a junction) and a finite number of particles with Hamiltonian H . The system is prepared in an initial state $|\Psi_0\rangle$ which is an eigenstate of some Hamiltonian $H_0 \neq H$. From a physical point of view this initial state may represent, e.g., a charge, particle, or energy imbalance between the two finite electrodes that sandwich the junction. The system is then left to evolve from this initial condition under the dynamics of H , and the average current across some surface or any other observable is monitored in time. The dynamics considered here may be considered as quantum quenches [38, 39]. Note that, even if we assume the two electrodes biased as in the Landauer formalism, in this closed-system approach it is not at all obvious that the average current establishes any (quasi-)steady state in the course of time [11, 19, 40].

A. Implementation of the MCF

We adopt the implementation of the micro-canonical formalism as discussed in Refs. [23, 24], which is an extension of the scheme proposed in Ref. [20]. One advantage of this extended scheme is that the dynamics of particle density fluctuations, entanglement entropy, and density distributions can be easily monitored. We consider a one-dimensional Hamiltonian $H = H_L + H_R + H_C$, where $H_{L/R}$ is a lattice of $N/2$ sites. The system is filled with $N/2$ two-component fermions (with equal number in each species). In the tight-binding approximation we choose

$$H_{L/R} = -\bar{t} \sum_{\langle ij \rangle, L/R} c_i^\dagger c_j + E_{L/R} \sum_{i \in L/R} c_i^\dagger c_i. \quad (6)$$

Here $\langle ij \rangle$ denotes nearest-neighbor pairs and we suppress the spin index, and explicitly state where a summation over the spin is performed in our results. Here we only consider quadratic Hamiltonians. In the presence of other interaction terms, one may need to consider approximate methods [26].

We consider two possible ways to set the system out of equilibrium. In the first scenario the system is initially prepared in the ground state of the unbiased Hamiltonian H_0 with $E_L = E_R = 0$ and then it evolves according to a biased Hamiltonian H . All conclusions in this work remain unchanged if we instead prepare the system in the ground state of the biased H and then let it evolve according to the unbiased H_0 . In other words, there is a correspondence between a particle imbalance and an energy imbalance for the systems we consider. In the second scenario two initially disconnected lattices are connected, where one can not swapped the roles of H and H_0 . We remark that the first scenario is closely related to the studies of Ref. [41] where photons are introduced to adjust the onsite energy of atoms in certain parts of the lattice. The second scenario is relevant to the case where an optical barrier separating the lattice into two parts is lifted [24].

For the weak-link case $H_C = -\bar{t}'(c_{N/2}^\dagger c_{N/2+1} + c_{N/2+1}^\dagger c_{N/2})$, where $0 \leq \bar{t}' \leq \bar{t}$, while for the central-site case $H_C = E_C c_{N/2+1}^\dagger c_{N/2+1} - \bar{t}(c_{N/2}^\dagger c_{N/2+1} + c_{N/2+1}^\dagger c_{N/2}) - \bar{t}(c_{N/2+1}^\dagger c_{N/2+2} + c_{N/2+2}^\dagger c_{N/2+1})$. For time $t < 0$, $E_{L/R} = 0$ and the system is in the ground state of H_0 . For $t > 0$ we set $E_L = \mu_B/2$ and $E_R = -\mu_B/2$ and let the system evolve. Figure 1 illustrates this process for the weak-link case. A uniform chain with $\bar{t}' = \bar{t}$ in the weak-link case has been shown to have a quasi steady-state current (QSSC) at a small bias [20] for a system as small as $N = 60$. The QSSC is defined as a plateau in the current as a function of t and it usually spans the range $(N/4)t_0 \leq t \leq (N/2)t_0$. In the thermodynamic limit with finite filling, the QSSC becomes a steady current [24]. In contrast, noninteracting bosons in their ground state do not support a QSSC [23, 24]. The dependence of the magnitude of the QSSC on the initial filling was discussed in Refs. [23, 24] and here we consider the case with $N_p/N = 1/2$, where N_p denotes the number of particles in the system, unless specified otherwise.

To gain more insight into the dynamics of the system, we write down the correlation matrix $C(t)$ with elements $c_{ij}(t) = \langle GS_0 | c_i^\dagger(t) c_j(t) | GS_0 \rangle$, where $|GS_0\rangle$ denotes the ground state of H_0 , and derive the current and entanglement entropy from it. One can use unitary transformations $c_j = \sum_k (U_0)_{jk} a_k$ and $c_j = \sum_k (U_e)_{jk} d_k$ to rewrite H_0 and H as

$$H_0 = \sum_k \epsilon_k^0 a_k^\dagger a_k; \quad H = \sum_p \epsilon_p^e d_p^\dagger d_p. \quad (7)$$

Here ϵ_k^0 and ϵ_p^e are the energy spectra of H_0 and H , respectively. The initial state is then $|GS_0\rangle = (\prod_{k=1}^{N/2} a_k^\dagger) |0\rangle$, where $|0\rangle$ is the vacuum. From the equation of motion $i(d c_j(t)/dt) = [c_j(t), H]$ it follows $c_j(t) = \sum_p (U_e)_{jp} d_p(0) \exp(-i\epsilon_p^e t)$. The initial correlation functions are $\langle GS_0 | a_k^\dagger(0) a_{k'}(0) | GS_0 \rangle = \theta(N/2 - k) \delta_{k,k'}$ since fermions occupy all states below the Fermi energy, where $\theta(N/2 - k)$ is 1 if $k \leq N/2$, and 0 otherwise. Then it follows

$$c_{ij}(t) = \sum_{p,p'=1}^N (U_e^\dagger)_{pi} (U_e)_{jp'} D_{pp'}(0) e^{i(\epsilon_p^e - \epsilon_{p'}^e)t}; \quad (8)$$

$$D_{pp'}(0) = \sum_{m,m'=1}^N \sum_{k=1}^{N/2} (U_e^\dagger)_{p'm'} (U_0)_{m'k} (U_0^\dagger)_{km} (U_e)_{mp}.$$

Here $D_{pp'}(0) \equiv \langle GS_0 | d_p^\dagger(0) d_{p'}(0) | GS_0 \rangle$.

B. Current, entanglement entropy, and particle fluctuations

The current flowing from left to right for one species is $I = -\langle d\hat{N}_L(t)/dt \rangle$, where $\hat{N}_L(t) = \sum_{i=1}^{N/2} c_i^\dagger(t) c_i(t)$. It can be shown that for the Hamiltonian considered here, $I = 4\bar{t}' \text{Im}\{c_{(N/2),(N/2+1)}(t)\}$, where a factor of 2 for the two spin components is included. This is equivalent to the expectation value of the current operator $\hat{I} = -i\bar{t}'(c_{N/2}^\dagger c_{N/2+1} -$

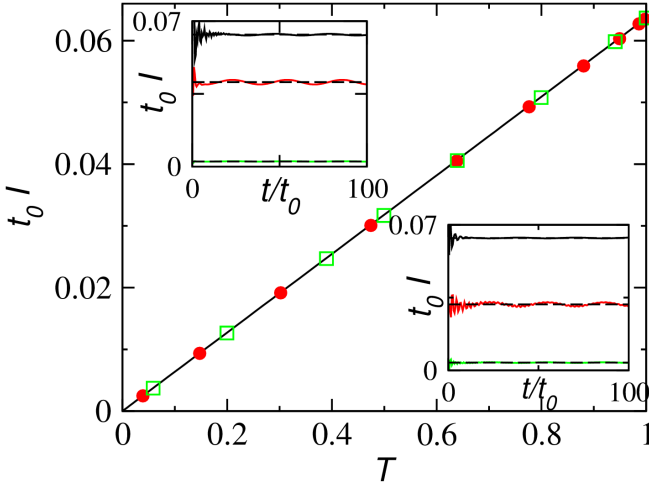


Figure 3. (Color online) The current from the Landauer formula for the weak-link case, Eq. (4), (black line) and the currents in the quasi-steady states of the micro-canonical simulations for the weak-link case (red circles) and the central-site case (green squares) as a function of the transmission coefficient $T = T(E = 0)$. Insets: Currents as a function of time from the micro-canonical simulations (solid lines; the dashed lines represent the Landauer value). The upper (lower) one corresponds to the weak-link (central-site) case. From top to bottom for the upper inset: $\bar{t}/\bar{t} = 1.0, 0.5, 0.1$ and for the lower inset: $E_C/\bar{t} = 0, 2, 8$. Here $\mu_B = 0.2\bar{t}$ and $N = 512$.

$c_{N/2+1}^\dagger c_{N/2}$). The MCF can be generalized to include finite-temperature effects in the initial state [23], but here we focus on the ground state.

Figure 3 compares the current predicted by the Landauer formula for the weak-link case, Eq. (4) to the simulations using the MCF for the weak-link as well as the central-site cases with $\mu_B = 0.2\bar{t}$. In the limit where $\mu_B \rightarrow 0$, the Landauer formulas for the central-site case, Eq. (5), produces results that fully agree with the results from the weak-link case, Eq. (4). When μ_B is finite, the two cases differ by a negligible amount due to the slightly different $T(E)$. One can see that the currents from the MCF agree well with that from the Landauer formula.

The entanglement entropy between the left and right halves, s , for one species at time t can be evaluated as follows [18]. We define a $(N/2) \times (N/2)$ matrix $M = P_L C(t) P_L$ with elements M_{ij} , where the projection operator $P_L = \text{diag}(\mathbf{1}_{N/2}, \mathbf{0}_{N/2})$. Then the entanglement entropy can be obtained from the expression

$$s = -\text{Tr}[M \log M + (1 - M) \log(1 - M)]. \quad (9)$$

The Hermitian matrix M_{ij} has eigenvalues v_i , $i = 1 \dots N/2$. Then

$$s(t) = \sum_{i=1}^{N/2} [-v_i \log(v_i) - (1 - v_i) \log(1 - v_i)]. \quad (10)$$

We use log base 2, as is convention. This expression may be further simplified by using approximations from the semi-classical FCS [18] and will be discussed later on. The noninteracting fermions studied here may be regarded as a limiting

case of a XXZ spin chain, whose entanglement entropy (due to the dynamics of magnetization) has been studied in Ref. [42].

Now we derive the full quantum-mechanical expressions for the equal-time number fluctuations of the left half lattice. Let $\hat{n}_i = c_i^\dagger c_i$ and $\hat{N}_L = \sum_{i=1}^{N/2} \hat{n}_i$. Then the number of particles in the left part is $N_L = \langle \hat{N}_L \rangle = \sum_{i=1}^{N/2} c_{ii}$. We define the equal-time number fluctuations of the left half as

$$\Delta N_L^2 = \langle (\hat{N}_L - N_L)^2 \rangle = \langle \hat{N}_L^2 \rangle - N_L^2. \quad (11)$$

The moments of \hat{N}_L can be obtained from

$$\langle \hat{N}_L^2 \rangle = \sum_{i=1}^{N/2} \langle \hat{n}_i^2 \rangle + 2 \sum_{i < j}^{N/2} \langle \hat{n}_i \hat{n}_j \rangle \quad (12)$$

From Wick's theorem or exact calculations, $\langle \hat{n}_i^\alpha \rangle = \langle \hat{n}_i \rangle = n_i$ for all positive integer α , where $n_i = c_{ii}$. The other correlation functions can be obtained from Wick's theorem so that

$$\langle \hat{n}_i \hat{n}_j \rangle = n_i n_j - |\langle c_i^\dagger c_j \rangle|^2. \quad (13)$$

IV. SPATIAL RESOLUTION OF THE CURRENT IN MCF

We stress an important feature of the MCF formalism. One can see from Eq. (8) and its context that MCF monitors the dynamics in both energy basis and real space. In contrast, the Landauer formalism as shown in Eq. (1) only reveals information in the energy basis. The ability of the MCF to trace the dynamics in real space allows us to address a crucial question: How do particles from different sites contribute to the current?

To clearly demonstrate the importance of the information from the dynamics in real space, we consider a simplified initial condition where N lattice sites are divided into the left $N/2$ sites and the right $N/2$ sites with each left site occupied by one fermion and each right site empty. We consider a uniform lattice here with a tunneling coefficient \bar{t} . The corresponding correlation matrix is $c_{ij}(t=0) = \delta_{ij}$ if $1 \leq i, j \leq (N/2)$ and zero otherwise. Eq. (8) becomes

$$c_{ij}(t) = \sum_{m=1}^{N/2} \sum_{p,p'=1}^N (U_e^\dagger)_{pi} (U_e)_{jp'} (U_e^\dagger)_{mp} (U_e)_{p'm} e^{i(\epsilon_p^e - \epsilon_{p'}^e)t} \quad (14)$$

One important insight from this expression is that the index m traces the contribution from the initially filled m -th site on the left. Therefore in the current $I = -2\bar{t}\text{Im}(c_{N/2, N/2+1})$ it is meaningful to discuss where does the current come from as time evolves.

This simplified case, despite its compactness and clarity, is relevant to several situations realizable in experiments. Two potential examples are: (1) initially a large step-function bias is applied to a nanowire with a small energy bandwidth so that all mobile particles are driven to the left half and then the bias is removed to allow a current to flow, and (2) ultra-cold atoms are loaded in an optical lattice so that there is one atom per lattice site. Then a focus laser beam excites the atoms on the right half lattice so that they leave the lattice and create a vacuum region. The atoms on the filled left part will then

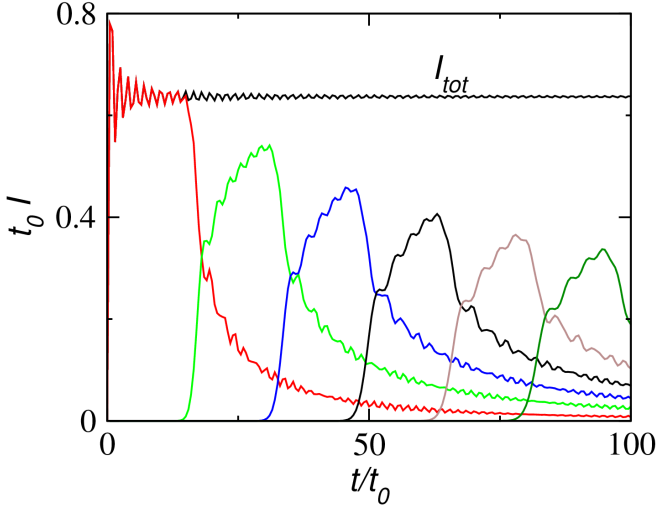


Figure 4. (Color online) Spatial decomposition of the contribution to the current. The black line labeled I_{tot} shows the current from an $N = 512$ lattice with the left half initially filled with one fermion per site. We plot the contributions from sections of 32 sites each to the left of the middle of the whole lattice and the corresponding currents show up in bursts. The bursts, from left to right on the plot, correspond to the current from the first, second, ..., sixth sections of 32 sites to the left away from the middle (the 256-th site).

flow to the right and build a current. Thus the physics of this simplified case is relevant to both our deeper understanding of transport phenomena and advances in experiments.

Figure 4 shows the total current of this case with $N = 512$ and clearly there is a quasi steady-state current. When we determine the contributions from each section of 32 lattices sites to the left of the middle (256-th site), each contribution comes in a burst following the previous burst from the section to its right. Thus the burst from the section of the 225-th site to the 256-th site crosses the middle first, followed by the burst from the section of the 193-th site to the 224-th sites, and so on, with each burst having a decaying tail. This succession of bursts gives a physical justification of the reason the semi-classical distribution assumed in FCS is binomial, and why other distributions can be excluded (see below). Each burst peak plus all the tails from previous bursts add up to maintain the observed quasi steady-state current. The MCF formalism thus provides more insights into how a quasi steady-state current forms and this is certainly beyond the scope of the Landauer's formalism. Since some spin chain problems can be mapped to fermions in 1D, our study is relevant to the dynamics of magnetization in these cases as well [43].

V. SEMI-CLASSICAL FCS FORMALISM

For two 1D non-interacting fermionic systems connected by a central barrier, it has been proposed [18] that an expression for the entanglement entropy can be derived from FCS assuming a binomial distribution of the transmitted particle

number. In linear response, it has the form

$$\frac{\Delta s}{\Delta t} = -2 \frac{\mu_B}{h} [T \log T + (1 - T) \log(1 - T)]. \quad (15)$$

Here, T is the transmission coefficient at the Fermi energy. The second moment of transmitted particle numbers, C_2 , is important because it may be inferred from shot-noise measurements. Moreover, the spectrum of current fluctuations through the barrier, P_{sn} , is related to C_2 by $P_{sn} = C_2/t$. Refs. [18] gives the prediction for P_{sn} :

$$P_{sn} = \frac{C_2}{t} = \frac{2\mu_B}{h} T(1 - T). \quad (16)$$

We will briefly review the derivations for these expressions.

In a semi-classical description, the second moment of transmitted particle numbers, C_2 , is equivalent to the number fluctuations of the left half of the system if the number of particles are conserved. This can be understood as follows. Let us assume that at time t there are N_{L0} particles on the left. At time $t + \Delta t$, if there are N_T particles passing through the barrier, the total number of particles on the left becomes $N_L = N_{L0} - N_T$. When N_{L0} is treated as a number, one has $C_2 = \langle N_T^2 \rangle - \langle N_T \rangle^2 = \langle N_L^2 \rangle - \langle N_L \rangle^2 = \Delta N_L^2$.

In a fully quantum-mechanical description, however, N_{L0} is an operator and the cross-correlation $\langle \hat{N}_{L0} \hat{N}_T \rangle \neq \langle \hat{N}_{L0} \rangle \langle \hat{N}_T \rangle$ may introduce corrections to the expression. In the micro-canonical formalism, the fully quantum-mechanical equal-time number fluctuations, ΔN_L^2 , can be monitored. We will compare this with the prediction of C_2 from the semi-classical formula Eq. (16) and see how important the quantum corrections are.

We summarize how the moments and entanglement entropy can be evaluated from semi-classical FSC [18]. The characteristic function (CF) of transmission of fermions of one species is $\chi(\lambda) = \sum_{n=-\infty}^{\infty} P_n e^{i\lambda n}$, where P_n is the probability of n fermions being transmitted. In terms of cumulants of FCS,

$$\log \chi(\lambda) = \sum_{m=1}^{\infty} \frac{(i\lambda)^m}{m!} C_m. \quad (17)$$

Importantly, the generating function is shown to be [18]

$$\chi(\lambda) = \det \left((1 - M + M e^{i\lambda}) e^{-i\lambda X} \right), \quad (18)$$

where $X = \exp(iHt)C(0)P_L \exp(-iHt)$ and P_L is the projection operator into the left-half lattice. Using $\det(AB) = \det(A) \det(B)$ and $\log \det(A) = \text{Tr} \log(A)$ one obtains

$$\log \chi(\lambda) = -i\lambda x + \log[\det(1 - M + M e^{i\lambda})], \quad (19)$$

where $x = \text{Tr}(X)$ and Tr denotes the trace. The matrix M can be diagonalized as $M = S D_M S^\dagger$, where $D_M = \text{diag}(v_1, \dots, v_{N/2})$ and S is a unitary matrix. Then we get the final expression

$$\log \chi(\lambda) = -i\lambda x + \log \prod_{j=1}^{N/2} (1 - v_j + v_j e^{i\lambda}). \quad (20)$$

The second cumulant can be obtained from

$$C_2 = \frac{\partial^2 \log \chi(\lambda)}{\partial (i\lambda)^2} \Big|_{\lambda \rightarrow 0} = \sum_{j=1}^{N/2} (v_j - v_j^2). \quad (21)$$

The entanglement entropy defined in Eq. (9) can be calculated as

$$s = - \int_0^1 dz \mu(z) [z \log z + (1-z) \log(1-z)]. \quad (22)$$

Here $z = 1/(1 - e^{i\lambda})$ and the spectral weight $\mu(z)$ is given by

$$\mu(z) = \frac{1}{\pi} \text{Im} \partial_z \log \chi(z - i0^+). \quad (23)$$

The CF of a binomial distribution with a transmitted probability T is $\chi(\lambda) = (1 - T + T e^{i\lambda})^N = (1 - T/z)^N$, where $N = 2\mu_B \Delta t / \hbar$ is the flux of incoming particles. The spectral weight is then

$$\begin{aligned} \mu(z) &= \frac{1}{\pi} \text{Im} \partial_z \log \left(1 - \frac{T}{z - i0^+} \right) \\ &= \mathcal{N} \frac{T}{z} \delta(z - T) \\ &= \mathcal{N} \delta(z - T). \end{aligned} \quad (24)$$

In this derivation we have used $1/(x - i0^+) = P(1/x) + i\pi\delta(x)$, $\delta(z(z-T)) = (1/z)\delta(z-T)$, and $(T/z)\delta(z-T) = \delta(z-T)$, where P denotes the Cauchy principal value. Then the entanglement entropy of Eq. (22) leads to the expression of Eq. (15). A similar calculation using Eq. (21) gives the expression of Eq. (16).

VI. ABSENCE OF MEMORY EFFECTS FOR NON-INTERACTING SYSTEMS

Before presenting a comparison of the MCF results with those of the Landauer formalism, we first investigate how sensitive the MCF results are to the time-dependence of the switch-on of the bias. This is important because in the Landauer formalism a steady state is assumed from the outset, while in the MCF a quasi-steady state develops in time and therefore its magnitude can be dependent on initial conditions and transient behavior of the bias.

So far we only considered a sudden quench so that μ_B is abruptly switched to its full value. The MCF can be applied to other scenarios beyond a sudden quench. Here we consider situations where μ_B is switched on at a finite rate and reaches its full value at time t_m . Here, we focus on the weak-link case and one has to monitor the dynamics of the correlation matrix by solving the equations of motion

$$\begin{aligned} i \frac{\partial \langle c_i^\dagger c_j \rangle}{\partial t} &= X - \frac{\mu_B}{2} \langle c_i^\dagger c_j \rangle_{i \in L} + \frac{\mu_B}{2} \langle c_i^\dagger c_j \rangle_{j \in L} + \\ &\quad \frac{\mu_B}{2} \langle c_i^\dagger c_j \rangle_{i \in R} - \frac{\mu_B}{2} \langle c_i^\dagger c_j \rangle_{j \in R}. \end{aligned} \quad (25)$$

Here, $X \equiv [\bar{t}' \delta_{i,N/2} + \bar{t}'(1 - \delta_{i,N/2})] \langle c_{i+1}^\dagger c_j \rangle + [\bar{t}' \delta_{i,N/2+1} + \bar{t}'(1 - \delta_{i,N/2+1})] \langle c_{i-1}^\dagger c_j \rangle - [\bar{t}' \delta_{j,N/2} + \bar{t}'(1 - \delta_{j,N/2})] \langle c_i^\dagger c_{j+1} \rangle -$

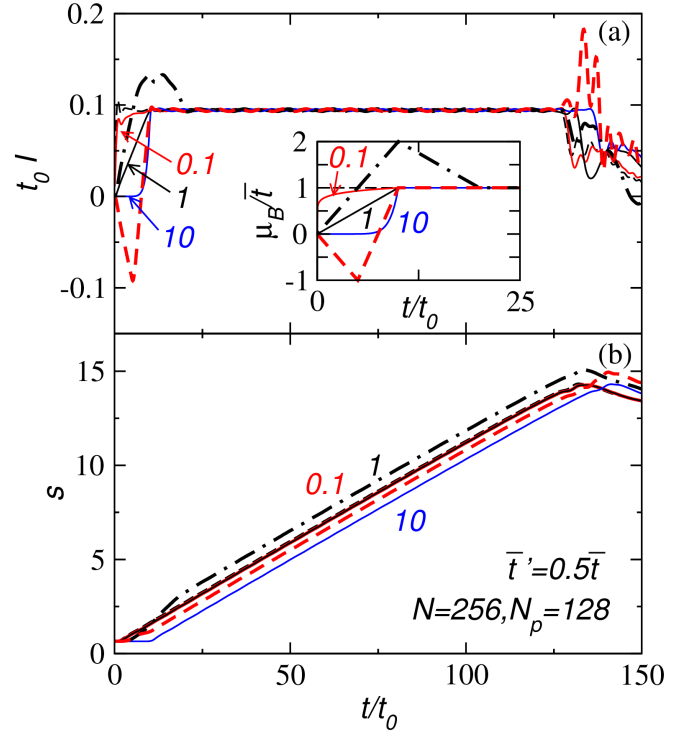


Figure 5. (Color online) (a) Current and (b) entanglement entropy for different time dependence of the bias $\mu_B = (t/t_m)^\alpha \bar{t}$ for $t < t_m$. Here $t_m = 10t_0$, $\bar{t}'/\bar{t} = 0.5$, $N = 256$ and $N_p = 128$. We show the results for $\alpha = 0.1, 1, 10$ labeled next to each curve along with the results from a sudden quench (dashed lines) and from a multi-step switching-on (dot-dash line).

$[\bar{t}' \delta_{j,N/2+1} + \bar{t}'(1 - \delta_{j,N/2+1})] \langle c_i^\dagger c_{j-1} \rangle$. The equations of motion are derived from $i(\partial \langle c_i^\dagger c_j \rangle / \partial t) = \langle [c_i^\dagger, H] c_j \rangle + \langle c_i^\dagger [c_j, H] \rangle$, where $[\cdot, \cdot]$ denotes the commutator of the corresponding operators. We assume that the dynamics of the two spins are identical and the initial condition is the same as that in the sudden-quench case.

Figure 5 shows the current and entanglement entropy from different cases with $\mu_B(t) = (t/t_m)^\alpha \bar{t}$ for $t < t_m$ and $\mu_B = \bar{t}$ for $t \geq t_m$. One can see that despite different transient behaviors, the currents reach the same magnitude when QSSCs emerge. Moreover, the slopes of the entanglement entropy are also the same in the regime where QSSCs emerge. We find the same conclusion when t_m is varied. Importantly, one may over-excite the system by tuning the bias *above* its final constant value, and yet this spike does not affect the height of the QSSC or the slope of the entanglement entropy as shown by the dot-dash lines in Fig. 5.

Our observations then suggest that there is no observable memory effect in the QSSC and entanglement entropy of non-interacting fermions driven by a step-function bias because those observables are not sensitive to the details of how the bias is turned on. However, the robustness of the QSSC against different time dependencies of the switch-on of the bias may not hold in the presence of interactions, and we leave this study for future work.

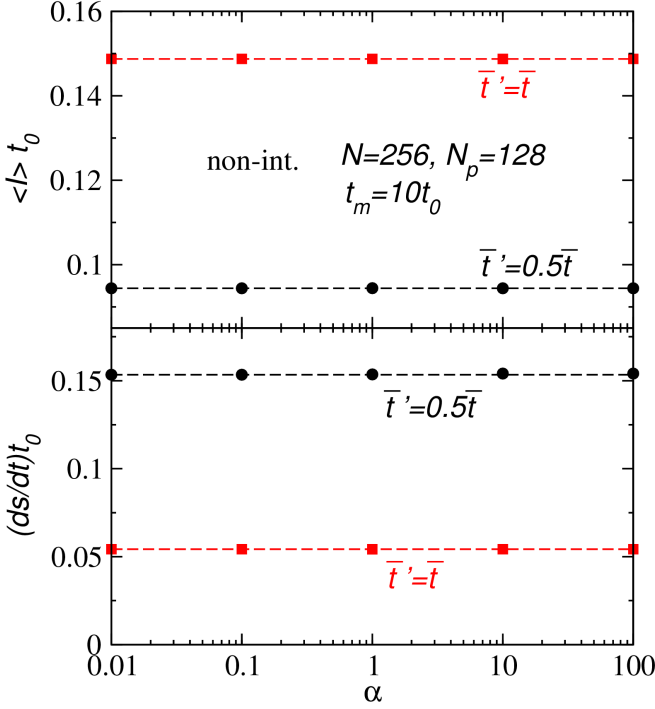


Figure 6. (Color online) (a) Averaged current (Eq. (26)) and (b) slope of the entanglement entropy for different time dependence of the bias $\mu_B(t/t_m)^{\alpha} \bar{t}$ for $t < t_m$. Here $t_m = 10t_0$, $\bar{t}'/\bar{t} = 0.5$ (black) and $\bar{t}'/\bar{t} = 1$ (red), $N = 256$ and $N_p = 128$. We show the results for $\alpha = 0.01, 0.1, 1, 10, 100$ along with the results from a sudden quench (dashed lines).

Figure 6 shows the averaged current

$$\langle I \rangle = \frac{1}{50t_0} \int_{50t_0}^{100t_0} dt I(t) \quad (26)$$

and the slope of s in the region $50t_0 \leq t \leq 100t_0$ for $\alpha = 0.01, 0.1, 1, 10, 100$ along with the results from a sudden quench. The results from those cases where the bias is turned on in a finite time t_m exhibit no observable deviation from the results from the case of a sudden quench. We choose $t_m = 10t_0$ and $N = 256$ with $N_p = 128$, but the conclusion holds for other parameters. Thus in the following we focus on the sudden-quench case when we compare the MCF and analytical formulas.

VII. COMPARISONS

Figure 7 shows the current, entanglement entropy, and number fluctuations of the weak-link case for selected values of \bar{t}'/\bar{t} . The currents clearly exhibit a quasi-steady state after a short transient time. We emphasize again that the steady-state current results from the quantum dynamics of the system and is not assumed *a priori*. The corresponding steady-state currents calculated from the Landauer formula, Eq. (1), are plotted on the same figure. The results from our simulations agree well with the predictions from Landauer formula. This

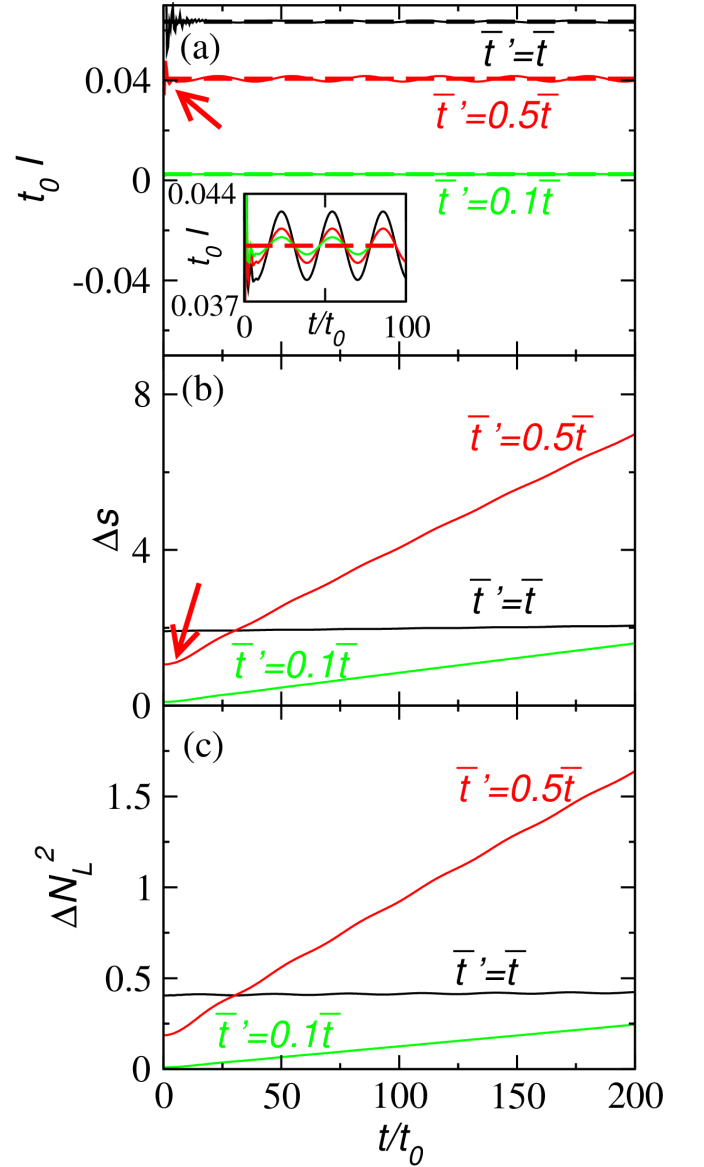


Figure 7. (Color online) (a) Current, (b) entanglement entropy, and (c) particle number fluctuations of the weak-link case with $\bar{t}'/\bar{t} = 1, 0.5, 0.1$ (labeled next to the corresponding curve). The dashed lines in (a) show the current predicted by Landauer formula, Eq. (1), with the corresponding parameters. The arrows point to the transient regime where the current fluctuates in (a) and the entropy deviates from the linear dependence in (b) for the case with $\bar{t}'/\bar{t} = 0.5$. The inset shows I for $N = 256, 512, 1024$ (from the largest oscillation amplitude to the smallest one) and the current predicted by Eq. (1) (dashed line) for $\bar{t}'/\bar{t} = 0.5$. Here $\mu_B = 0.2\bar{t}$ and $N = 512$.

agreement is in line with the observation that as the system approaches thermodynamic limit ($N \rightarrow \infty$ with finite filling), the microcanonical setup becomes indistinguishable from that in the Landauer formalism. For the case $\bar{t}' = \bar{t}$, we recover the quantized conductance, $G_0 = I/\mu_B = 2e^2/h$ (spin included). As expected, in the presence of a barrier ($\bar{t}' < \bar{t}$), the conductance is smaller than the quantized conductance. The suppression of the current by a weak central link was also

shown in Ref. [44]. We also test finite-size effects by comparing the currents from $N = 256, 512, 1024$ with the prediction from Landauer formula in the inset of Fig. 7. One can see that while the oscillation amplitude decreases with increasing system size, the average currents of the three different sizes all agree well with the analytical result. For the central-site case we found similar results.

When the link strength \bar{t}' or the central-site energy E_C is tuned, the transmission coefficient $T(E)$ changes accordingly. Figure 3 compares the quasi steady-state currents from Landauer formula (black line) and from micro-canonical simulations of the weak-link case (red circles) and the central-site case (green squares) as a function of the transmission coefficient $T = T(E = 0)$. The three results agree well and this supports the expectation that the Landauer formalism provides reasonable predictions. However, we will see that the agreement does not hold when we study the distributions on the two sides of the junction.

The entanglement entropy is expected to be linear in time and our results support this claim. We found that the slope of $\Delta s = s - s(\mu_B = 0)$ is proportional to μ_B as predicted in Eq. (15). For different values of \bar{t}'/\bar{t} , we test the predictions from the two formulas. From Fig. 2 we find that in the range $-\mu_B/2 \leq E \leq \mu_B/2$ the variation of $T(E)$ is within 3% for all cases we studied so we take $T(E = 0)$ as the transmission coefficient in our evaluation of Eq. (15).

The slope of the entanglement entropy from micro-canonical formalism and the predictions from Eq. (15) are shown in Figure 8 for $\mu_B/\bar{t} = 0.1$ and 0.2 . One can see that our results agree well with Eq. (15) for all values of T and this implies that the distribution of tunneling particles may be approximated by a binomial form as assumed in Ref. [18]. In the derivation of Eq. (15) and in our simulation, fermions of different spins tunnel independently and do not generate spin-entangled states. The entanglement entropy comes from the correlation of partially tunneled and partially reflected wavefunctions of particles.

We notice that the transient time, which is defined as the initial time interval during which the system has not reached a quasi-steady state, seems to differ in $I(t)$ and $s(t)$ (as illustrated in Fig. 7). During the transient time, the currents fluctuate violently while the entropy exhibit a downward bending. From our simulations we found that the transient time for $s(t)$ is three times larger than that for $I(t)$ and this relation seems to be insensitive to the system size.

To investigate how FCS depends on the underlying probability distribution, we study the behavior of Eq. (15) when a Gaussian (continuous) distribution is implemented. To make connections with the original binomial distribution, we choose the mean $m = \mathcal{N}T$ and the variance $\sigma^2 = \mathcal{N}T(1 - T)$ to match those of the binomial distribution. The CF is $\chi(\lambda) = \exp(im\lambda - \frac{1}{2}\sigma^2\lambda^2)$. A change of variable $z = 1/(e^{i\lambda} - 1)$ gives $\chi(z) = \exp(\mu \log(1 - \frac{1}{z}) + \frac{1}{2}\sigma^2[\log(1 - \frac{1}{z})]^2)$. One then finds $\text{Im}\partial_z \log \chi(z) = \text{Im}[\frac{m}{z^2 - z} + \frac{\sigma^2}{z^2 - z} \log(1 - \frac{1}{z})]$. When one changes z to $z - i0^+$ and uses the formula $1/(x - i0^+) = P(1/x) + i\pi\delta(x)$, the imaginary part of $1/(z^2 - z)$ does not contribute to the integral of s because the delta function $\delta(z^2 - z)$ can only be satisfied at $z = 0, 1$ but those points do

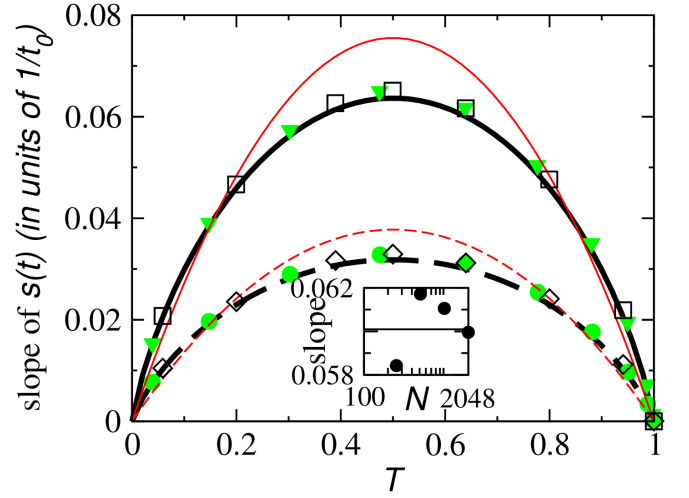


Figure 8. (Color online) Comparison of the slope of $s(t)$ from Eq. (15) (red) and simulations (symbols). Here the results for $\mu_B/\bar{t} = 0.1$ are represented by the dashed line, circles (weak-link), and diamonds (central-site) while those for $\mu_B/\bar{t} = 0.2$ are represented by the solid line, triangles (weak-link), and squares (central-site). We choose $N = 512$ and $T = T(E = 0)$. The thin red solid and dashed lines shows the results for a Gaussian distribution, Eq. (27), for $\mu_B/\bar{t} = 0.2$ and 0.1 . Inset: The slopes (in units of t_0^{-1}) from different system sizes $N = 256, 512, 1024, 2048$ showing the convergence to the semi-classical value for $\bar{t}'/\bar{t} = 0.5$ (solid line).

not have finite s . The only contribution in the spectral weight is thus $\mu(z) = \frac{1}{\pi} \frac{\sigma^2}{z^2 - z} \text{Im}[\log(1 - \frac{1}{z - i0^+})]$. One can show that $\text{Im}[\log(1 - \frac{1}{z - i0^+})] = \arg((z - 1)/z) = -\pi$ (the choice of the sign will be clear in a moment) for $0 < z < 1$. Thus the weight is $\mu(z) = -\frac{\sigma^2}{z^2 - z}$ which is positive for $0 < z < 1$. From $s = -\int_0^1 dz \mu(z) [z \log z + (1 - z) \log(1 - z)]$ [18] one gets $s = \alpha \sigma^2 = \alpha(2\mu_B/h)T(1 - T)\Delta t$. Thus

$$\frac{\Delta s}{\Delta t} = \alpha \left(\frac{2\mu_B}{h} \right) T(1 - T), \quad (27)$$

where $\alpha \approx 3.3$ is a numerical factor. In Figure 8 we show (in thin red lines) its values. It is clear that the data from the micro-canonical simulations can distinguish these distributions.

As the system size increases, the small oscillation on top of the linear increase of the entanglement entropy decreases. We found that this reduces the difference between the slope from fitting the results from the MCF and the slope predicted by the semi-classical FCS formalism. In the inset of Fig. 8 we show the slope from the MCF for $N = 256, 512, 1024, 2048$ with half-filling. One can see that as N increases the agreement improves. However, optical lattices in real experiments are of limited sizes so one may expect observable finite-size effects in experimental results.

Next we extract the slopes of ΔN_L^2 and compare the results with the slopes predicted from the semi-classical formula of the second cumulant, Eq. (16), in Figure 9. The slopes agree reasonably well, which implies that quantum corrections to the semi-classical formula are insignificant. More-

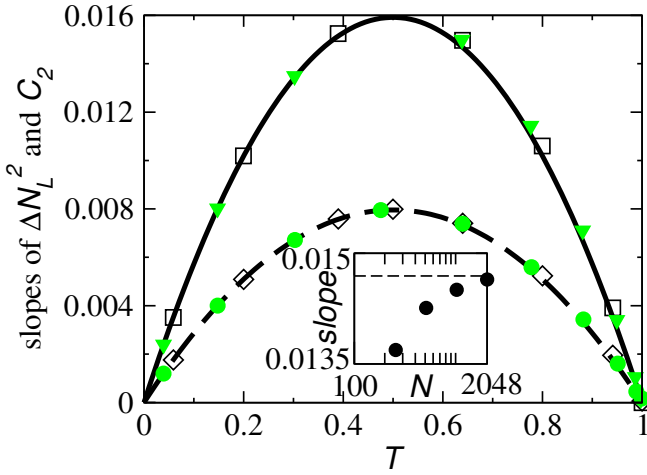


Figure 9. Comparison of the slopes (in units of t_0^{-1}) of ΔN_L^2 (symbols) and C_2 from Eq. (16) (curves). The circles (weak-link), diamonds (central-site), and dashed line correspond to $\mu_B/\bar{t} = 0.1$ while the triangles (weak-link), squares (central-site), and solid line correspond to $\mu_B/\bar{t} = 0.2$. Here $N = 512$ with half filling. Inset: The slope (in units of t_0^{-1}) of ΔN_L^2 for $N = 256, 512, 1024, 2048$ at half filling with $\bar{t}'/\bar{t} = 0.5$. The dashed line shows the result from Eq. (16).

over, we have compared the third and fourth moments with the quantum-mechanical fluctuations of the corresponding order. The results from micro-canonical simulations show observable deviations from those from semi-classical FCS in the fourth order but not in the third order. The slight difference between our results and the results from semiclassical FCS in Fig. 9 is due to finite-size effects. We have checked our results for larger system sizes and the result converges to the FCS prediction, as shown in the inset of Fig. 9.

So far the MCF agree reasonably with Landauer formalism and FCS. Now we will show several interesting phenomena associated with the finite size and conservation laws of isolated systems such as cold atoms. We first study the particle distribution functions on the left and the right sides. This can be done by first projecting the correlation matrix to the left (right) half uniform lattice and obtaining $M_L = P_L C P_L$ and $M_R = P_R C P_R$. Next we find the eigenvalues and the corresponding unitary transformations of H_L and H_R (with the biases on) so that $H_{L/R} = U_{L/R} D_{L/R} U_{L/R}^\dagger$, where $D_{L,R} = \text{diag}(\epsilon_{L/R,1}, \dots, \epsilon_{L/R,N/2})$. Then we construct the correlation matrix in energy space and get $\tilde{D}_{qq'}^{L/R} = \sum_{i,j \in L/R} (U_{L/R}^\dagger)_{qi} (U_{L/R})_{jq'} (M_{L/R})_{ij}$. For each eigenvalue $\epsilon_{L/R,q}$, the occupation number is given by $n_{L/R}(\epsilon_{L/R,q}) = \tilde{D}_{qq}^{L/R}$. In Fig. 10 we show the particle distributions for the weak-link case with $\bar{t}' = 0.5\bar{t}$ and $\bar{t}' = \bar{t}$ at $t = t_0, 100t_0$, and $200t_0$ for $N = 512$ with the system initially half-filled and $\mu_B = 0.2\bar{t}$. The particle distributions for the central-site case with similar parameters are shown in Fig. 11.

Clearly, the particle distributions on both sides vary dynamically but they evolve in a coordinated fashion so that the current across the junction remains constant for a long period

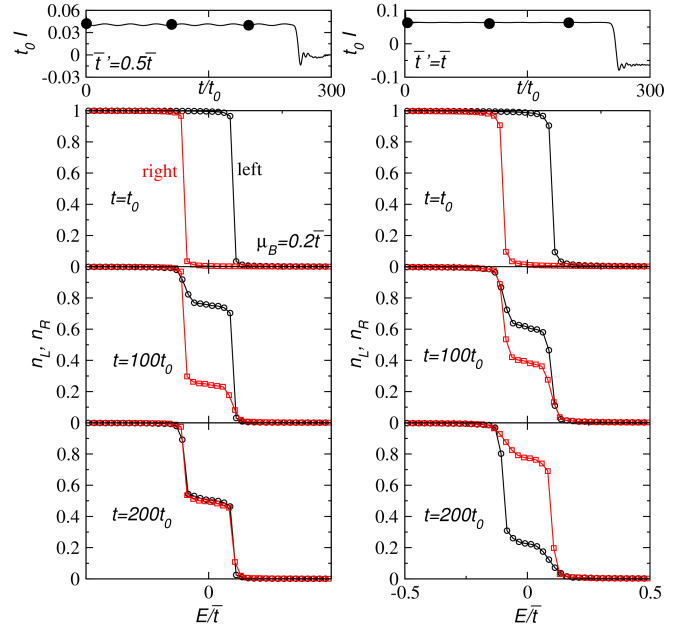


Figure 10. (Color online) The distribution function of the weak-link case with $\mu_B = 0.2\bar{t}$ and $\bar{t}' = 0.5\bar{t}$ (left column) and $\bar{t}' = \bar{t}$ (right column). From top to bottom, $t = t_0, 100t_0$, and $200t_0$. Here, $N = 512$ (with the lattice initially half-filled) and the quasi-steady state current persists to $240t_0$.

of time. This is different from the picture behind the Landauer formula. In Landauer formula the distributions on the left (right) half lattice are fixed at f_L (f_R) and a constant tunneling constant T determines the rate at which particles move across the junction. On the other hand, for a finite system, the particle distributions must evolve with time. If Eq. (1) is naively used in this case, one may expect that the current decays with time because the difference between the distributions, $f_L(E) - f_R(E)$, should be a decreasing function when particles are flowing from the left to the right. In contrast, a plateau in the current emerges in the full quantum dynamics. Even more surprisingly, there exists a time interval when a QSSC still flows from left to right, yet the right lattice has more particles, as shown in the bottom right panels of both Figs. 10 and 11 (for $t = 200t_0$) [45]. This highlights that this is a highly correlated state that allows the QSSC to persist. We will see in the next section this is due to causality and the finite speed of propagation of information, and thus is analogous to the light cone in special relativity.

There are recent proposals for designing batteries for atomtronic devices [8]. However, an important message from our study is that an isolated quantum system can maintain a quasi steady-state current in many cases. The quasi-steady state, as we demonstrated, is maintained by internal dynamics so a battery may not be the only way for generating a steady current in atomtronic devices, one could instead engineer an appropriate initial state that will induce a QSSC.

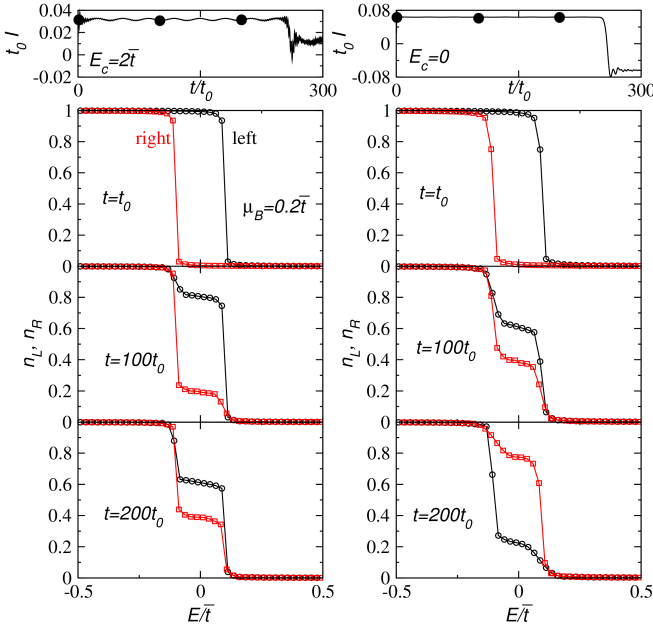


Figure 11. (Color online) The distribution function of the central-site case with $\mu_B = 0.2\bar{t}$ and $E_c = 2\bar{t}$ (left column) and 0 (right column). From top to bottom, $t = t_0$, $100t_0$, and $200t_0$. Here, $N = 512$ and the quasi-steady state current persists to $t = 240t_0$.

VIII. LIGHT-CONE OF WAVE PROPAGATION

In the last section, we saw that a QSSC can continue to flow even when the particle imbalance would indicate otherwise. This effect is due to the finite speed of information. Recent experimental studies [3, 46] have shown that the density profile exhibits a “light cone” as an atomic cloud expands, and there are ongoing theoretical studies to support this fact [47]. We can see this effect within the MCF (one of the many advantages of this formalism). We monitor the real-time dynamics of the density and current profiles for noninteracting fermions in a uniform lattice driven out of equilibrium by (1) a step-function potential as shown in Fig. 1, and (2) a sudden removal of atoms on the right-half lattice as discussed in Ref. [23]. The time evolution of the first case is shown in Figure 12 and that of the second case is shown in Fig. 13. In both cases one can see clearly a “light cone” within which the motion of atoms are confined. The propagation speed is limited by the Fermi velocity, which for filling f is $v_F = 2 \sin(f\pi)/t_0$. For $N = 512$ at half filling ($N_p = 256$), it takes about $128t_0$ for the wave front to reach the boundary and reflect back. Around $256t_0$ the two wave fronts propagating in the opposite directions meet again in the middle. That is when the current stops showing the quasi steady-state behavior. This applies to both cases, as shown in Fig. 12(c) and (d) and Fig. 13(c) and (d). This explains the paradoxical behavior of the QSSC flowing counter to the particle imbalance. This happens because the information regarding the population imbalance still has not been carried to the junction region where the current is being monitored.

For the quarter filling ($N_p = 128$), if the wave front propa-

gates at the speed of the corresponding Fermi velocity $\sqrt{2}/t_0$, it takes about $181t_0$ for the wave front to reach the boundary and the two wave fronts meet again at around $362t_0$. Although the main body of the wave propagates at this speed, there are “leaks” of the wave which propagate at speed higher than $\sqrt{2}/t_0$ but they are limited by the maximal Fermi velocity $2/t_0$, as shown in Figs. 12 and 13. This “leaking” behavior is more prominent for the case of a sudden removal of half of the particles at higher filling. As shown in Fig. 13(e) and (f), for initial $(3/4)$ filling there is significant fraction of the wave propagation at $2/t_0$. For the step-function bias case (Fig. 12(e) and (f)), the main wave propagates at $\sqrt{2}/t_0$ and again the leak propagates at higher speed (limited by $2/t_0$). We also found that adding a weak central link or a central site with different onsite energy only decreases the magnitude of the current, but the speed of wave-front propagation remains the same for the same initial filling.

IX. KUBO FORMALISM

In order to connect the microcanonical and Landauer approaches, we apply leading order perturbation theory on finite systems by way of the Kubo formula [11, 48, 49]

$$\langle A(t) \rangle = \langle A \rangle_0 - i \int_0^t dt' \langle [\hat{A}(t), \hat{H}'(t')] \rangle \quad (28)$$

for the observable A . Here, $\hat{O} = e^{iH_0 t} O e^{-iH_0 t}$ indicates an operator in the interaction picture, H' is the perturbing Hamiltonian, and $\langle O \rangle_0$ indicates an average with respect to the initial state. For all practical purposes, here we use the wavefunctions of finite-size systems without taking the thermodynamic limit commonly employed in solid-state systems. We will consider a one-dimensional lattice set out of equilibrium by connecting two initially disconnected halves with a weak link or by the application of a bias to an initially connected system, as shown in Fig. 1.

A. Connecting the L and R lattices

The initial Hamiltonian is

$$H_0 = H_L + H_R, \quad (29)$$

where

$$H_L = - \sum_{\langle i,j \rangle} \bar{t} c_i^\dagger c_j + \mu_L \sum_i c_i^\dagger c_i \quad (30)$$

and

$$H_R = - \sum_{\langle i,j \rangle} \bar{t} d_i^\dagger d_j - \mu_R \sum_i d_i^\dagger d_i. \quad (31)$$

The left and the right lattices are both finite lattices of length N with non-periodic (“open”) boundary conditions. We consider the ground state of H_L and H_R fixed at half filling –

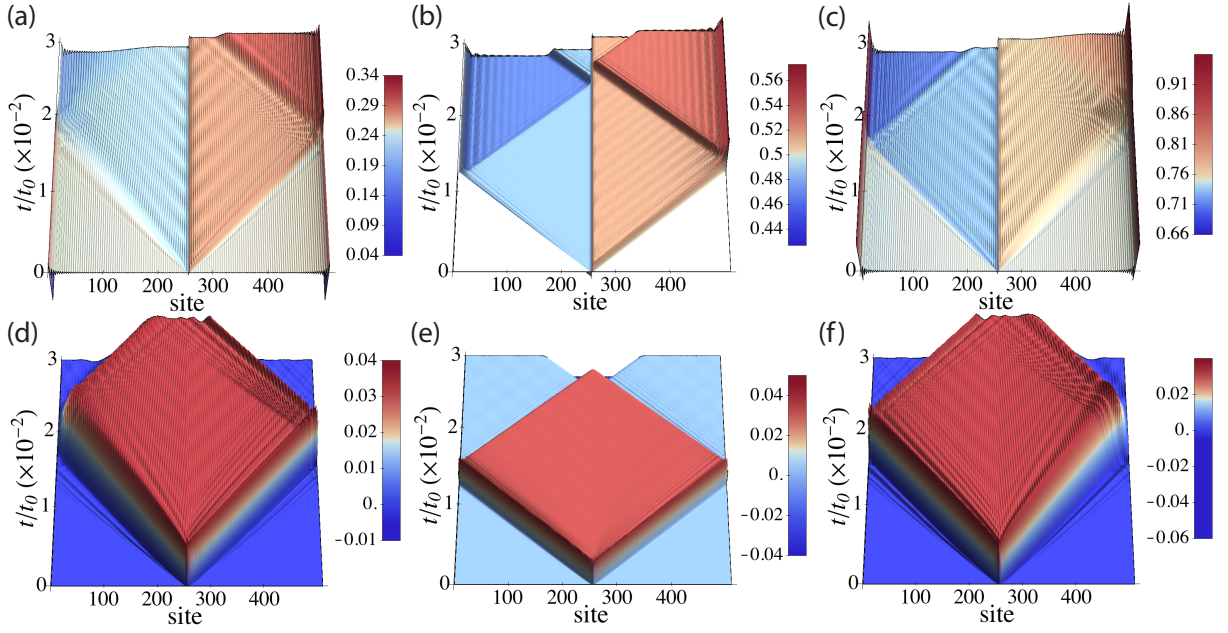


Figure 12. (Color online) The density profiles (top row) and current profiles (bottom row) for a uniform chain driven out of equilibrium by a step-function bias $\mu_B = 0.2\bar{t}$. Here $N = 512$ with $N_p = 128$ ((a) and (d)), $N_p = 256$ ((b) and (e)), and $N_p = 384$ ((c) and (f)). The Fermi velocity for half filling is $(2/t_0)$ and that for $(1/4)$ or $(3/4)$ filling is $(\sqrt{2}/t_0)$.

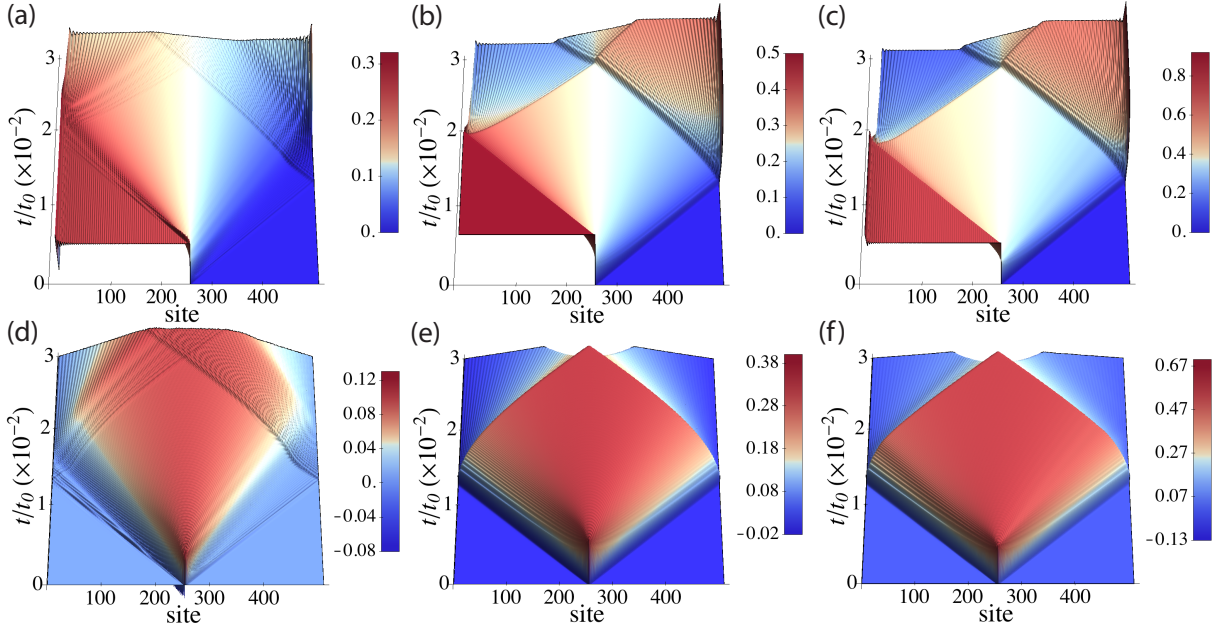


Figure 13. (Color online) The density profiles (top row) and current profiles (bottom row) for a uniform chain driven out of equilibrium by suddenly blowing away particles on the right half. Here $N = 512$ with initial particle number $N_p = 128$ for (a) and (d), $N_p = 256$ for (b) and (e), and $N_p = 384$ for (c) and (f).

the bias can be thought of as added simultaneously with the connection of the two lattices. The diagonalization of the left lattice is performed by $c_j = \sum_k U_{jk} a_k$ with $U_{jk} = \sqrt{2/(N+1)} \sin(jk\pi/(N+1))$ and $k = 1, \dots, N$, yielding $H_L = \sum_k \epsilon_k^L a_k^\dagger a_k$ and $\epsilon_k^L = -2\bar{t} \cos(k\pi/(N+1)) + \mu_L$. Similarly for the right lattice, using $d_j = \sum_k U_{jk} b_k$ gives

$$H_R = \sum_k \epsilon_k^R b_k^\dagger b_k \text{ and } \epsilon_k^R = -2\bar{t} \cos(k\pi/(N+1)) + \mu_R.$$

At $t = 0$, the lattices are connected by the perturbing Hamiltonian

$$H' = g\bar{t} (c_1^\dagger d_1 + d_1^\dagger c_1), \quad (32)$$

where $g = \bar{t}'/\bar{t}$. Note that the numbering of the sites in both

lattices starts from the interface sites. The current is the quantity of interest, hence we will take

$$A = g\bar{t}c_1^\dagger d_1, \quad (33)$$

where A gives the hopping between the two halves of the lattice, i.e., c_1 acts on the interface site on the left lattice and d_1 on the interface site of the right lattice. This will give the current through $I(t) = -2\text{Im}\langle A(t) \rangle$.

The interaction picture operators are

$$\hat{A}(t) = g\bar{t}^2 \sum_{k,k'} U_{k1}^\dagger U_{1k'} e^{i(\epsilon_k^L - \epsilon_{k'}^R)t} a_k^\dagger b_{k'} \quad (34)$$

and

$$\hat{H}'(t') = \left(\hat{A}(t') + \hat{A}^\dagger(t') \right). \quad (35)$$

Putting these into Eq. (28) and using that $\langle A \rangle_0 = 0$ for two initially disconnected lattices, we obtain

$$\langle A(t) \rangle = g^2 \bar{t}^2 \sum_{k,k'} |U_{k1}|^2 |U_{1k'}|^2 \frac{n_k - n_{k'}}{\epsilon_k^L - \epsilon_{k'}^R} \left(1 - e^{i(\epsilon_k^L - \epsilon_{k'}^R)t} \right). \quad (36)$$

The current is then

$$\begin{aligned} I(t) &= -2\text{Im}\langle A(t) \rangle \\ &= 2g^2 \bar{t}^2 \sum_{k,k'} |U_{k1}|^2 |U_{1k'}|^2 \frac{n_k - n_{k'}}{\epsilon_k^L - \epsilon_{k'}^R} \sin[(\epsilon_k^L - \epsilon_{k'}^R)t]. \end{aligned} \quad (37)$$

When the L and R lattices are half filled, this double sum will be nonzero when either $k \leq N/2$, $k' > N/2$ or $k > N/2$, $k' \leq N/2$.

To simplify the expressions and show the correspondence with Landauer, we take the semi-infinite limit for the left and right lattices obtaining

$$\begin{aligned} I(t) &= \frac{8g^2 \bar{t}^2}{\pi^2} \int_0^\pi dk \int_0^\pi dk' \sin^2 k \sin^2 k' \\ &\quad \times \frac{n_k - n_{k'}}{\epsilon_k - \epsilon_{k'} + \mu_B} \sin[t(\epsilon_k - \epsilon_{k'} + \mu_B)], \end{aligned}$$

where $\epsilon_k = -2\bar{t} \cos k$ and $\mu_B = \mu_L - \mu_R$. At this point, we have made no assumption about the strength of the bias, the filling, or the temperature. We will now restrict ourselves to the case of half filling and zero temperature.

The two contributions to this expression give the forward and backward currents, integrating over energy instead of wave vector,

$$\begin{aligned} I_{\rightarrow}(t) &= \frac{2g^2 \bar{t}}{\pi^2} \int_{-2}^0 d\epsilon \int_0^2 d\epsilon' \left(1 - \frac{\epsilon^2}{4} \right)^{1/2} \left(1 - \frac{\epsilon'^2}{4} \right)^{1/2} \\ &\quad \times \frac{\sin[t(\epsilon - \epsilon' + \mu_b)/t_0]}{\epsilon - \epsilon' + \mu_b} \end{aligned}$$

and

$$\begin{aligned} I_{\leftarrow}(t) &= \frac{2g^2 \bar{t}}{\pi^2} \int_0^2 d\epsilon \int_{-2}^0 d\epsilon' \left(1 - \frac{\epsilon^2}{4} \right)^{1/2} \left(1 - \frac{\epsilon'^2}{4} \right)^{1/2} \\ &\quad \times \frac{\sin[t(\epsilon - \epsilon' + \mu_b)/t_0]}{\epsilon - \epsilon' + \mu_b}. \end{aligned}$$

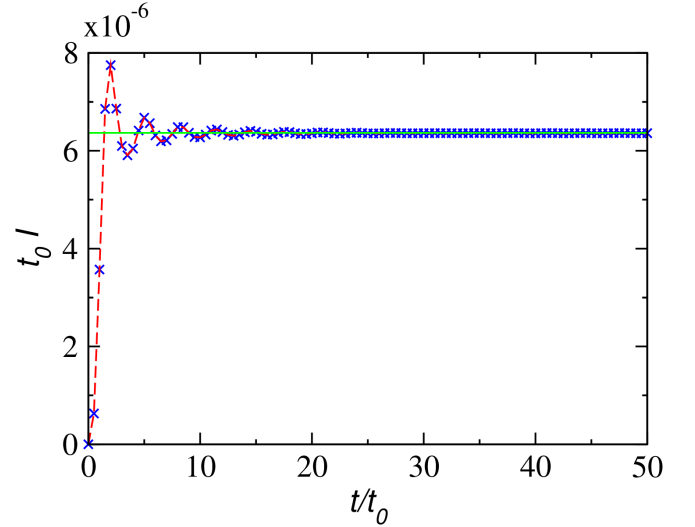


Figure 14. (Color online) Current versus time for connection-induced transport. The Kubo result (blue crosses) compares very well with the exact microcanonical method (red, dashed line), with both approaching the steady-state current (green, dashed line) for long times. Here, the lattice is of length 1600 sites, the bias is $\mu_B/\bar{t} = 1/10$, and the strength of the weak link is $g = 1/100$.

Here, $\mu_b = \mu_B/\bar{t}$. As $t \rightarrow \infty$, the fast oscillating function $\sin(tx)/\pi x$ enforces $\epsilon' = \epsilon + \mu_b$. This latter equality can not be satisfied in the backward current as ϵ is positive and μ_b is also positive, but ϵ' is negative. Thus, only the forward current remains, giving

$$I = \frac{g^2 \bar{t}^2}{\pi} \int_{-\mu_b/2}^{\mu_b/2} d\epsilon \bar{g}_L \bar{g}_R \quad (38)$$

in the steady state and including the factor of two for spin.

Here, $\bar{g}_{L(R)} = \sqrt{4 - (\epsilon \mp \mu_b/2)^2}$ and the bias is applied symmetrically. The result is insensitive, though, to how the bias is applied – the left lattice can be shifted by μ_B and right lattice by 0, or the left by $\mu_B/2$ and the right by $-\mu_B/2$. This expression is valid for arbitrary bias and agrees with the Landauer expression, Eq. (4), to leading order in g . For small bias, one obtains

$$I \simeq \frac{4g^2 \bar{t}}{\pi} \mu_B. \quad (39)$$

Figure 14 shows the agreement of this expression with the exact microcanonical expression for finite-size systems.

This Kubo approach is firmly rooted in the microcanonical picture – we have a finite, closed system (the semi-infinite limit is taken only for convenience) set out of equilibrium. The resulting expressions separate out the short time behavior – due to forward and backward fluctuations at all energy scales – and the long time behavior – the QSSC – that emerges from just the forward current.

B. Applied bias across the L and R lattices

Let us now consider an initial Hamiltonian for a connected, homogeneous lattice of length $2N$

$$H_0 = - \sum_{\langle i,j \rangle} \bar{t} c_i^\dagger c_j. \quad (40)$$

We consider the ground state of H_0 fixed at half filling. The diagonalization is the same as above except with a lattice of length $2N$, $c_j = \sum_k U_{jk} a_k$ with $U_{jk} = \sqrt{2/(2N+1)} \sin(jk\pi/(2N+1))$ and $k = 1, \dots, 2N$, yielding $H_0 = \sum_k \epsilon_k a_k^\dagger a_k$ and $\epsilon_k = -2\bar{t} \cos(k\pi/(2N+1))$.

At $t = 0$, the lattices are perturbed by the Hamiltonian

$$H' = \frac{\mu_B}{2} \sum_{i \in L} c_i^\dagger c_i - \frac{\mu_B}{2} \sum_{i \in R} c_i^\dagger c_i, \quad (41)$$

which applies the step potential bias as shown in Fig. 1. The strength of the perturbation is the bias μ_B . The current between the two halves is of interest, and therefore we choose

$$A = \bar{t} c_N^\dagger c_{N+1}. \quad (42)$$

The interaction picture operator is

$$\hat{A}(t) = \sum_{k,k'} U_{kN}^\dagger U_{N+1k'} e^{i(\epsilon_k - \epsilon_{k'})t} \bar{t} a_k^\dagger a_{k'}. \quad (43)$$

After some work, one finds that the current is

$$\begin{aligned} I(t) &= -2\text{Im}\langle A(t) \rangle \\ &= \frac{2\mu_B \bar{t}}{(2N+1)^2} \sum_{\substack{k \text{ Even}, \\ k' \text{ Odd}}} F_{kk'} \frac{n_k - n_{k'}}{\epsilon_k - \epsilon_{k'}} \sin[t(\epsilon_k - \epsilon_{k'})], \end{aligned}$$

where

$$F_{kk'} = 2\bar{t} + \frac{4\bar{t}^2 - \epsilon_k \epsilon_{k'}}{\epsilon_k - \epsilon_{k'}}. \quad (44)$$

As $t \rightarrow \infty$, one can compute the steady state current, $I \simeq \mu_B \bar{t} / \pi$, which includes a factor of two for spins. This agrees with the Landauer expression, Eq. (3), expanded to the leading order of μ_B . Figure 15 shows the agreement of this expression with the exact microcanonical expression for finite-size systems. One may build connections between the Landauer formalism and the MCF via the use of non-equilibrium Green's functions [50]. The Kubo approach here, however, gives explicit expressions for the effect of the reservoirs for discrete systems and thus explicitly connects closed, finite systems and their thermodynamic limit.

X. CONCLUSION

In summary, we have discussed different theoretical viewpoints for quantum transport phenomena that may be studied in ultra-cold atoms. In particular, we have compared the

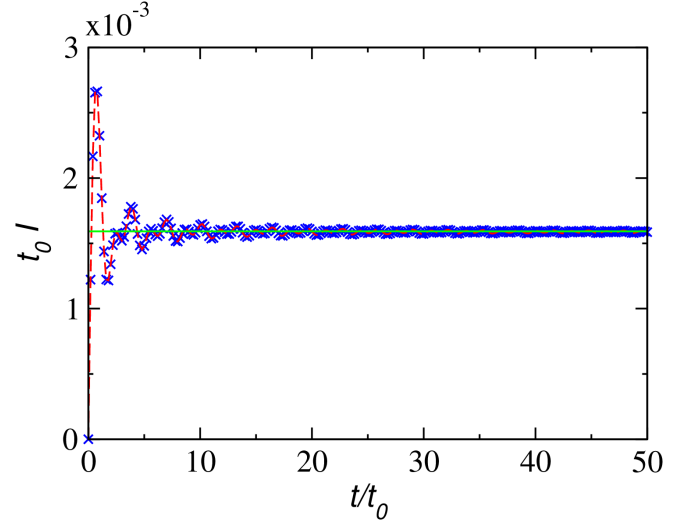


Figure 15. (Color online) Current versus time for bias-induced transport. The Kubo result (blue crosses) compares very well with the exact microcanonical method (red, dashed line), with both approaching the steady state current (green, dashed line) for long times. Here, the lattice is of length 1600 sites, the bias is $\mu_B/\bar{t} = 1/100$.

current, entanglement entropy, and number fluctuations from the Landauer approach, semi-classical FCS, and the micro-canonical formalism. In our study of two finite 1D lattices bridged by a junction, we found a quasi steady-state current from the quantum dynamics in the micro-canonical simulations. The magnitude of this quasi steady-state current agrees quantitatively with the value predicted by the Landauer approach. The underlying mechanisms, nevertheless, have been shown to be very different when the distributions of the two sides are analyzed. The distributions evolve in time and steadily deviate from Fermi-Dirac distributions even while the quasi steady-state current is maintained.

Our work points out several key issues when applying different formalisms to closed quantum systems such as ultra-cold atoms in optical lattices. Of particular importance is the confirmation, using the micro-canonical approach, that a quasi-steady state fermionic current can be established in a 1-D closed system for a finite period of time without the need of inelastic effects or interaction effects beyond mean field [20]. The magnitude of this non-interacting quasi-steady state current is independent of the way the bias is switched on. This also hints at the fact that the Landauer formalism may not be the best suited for the study of transport properties of these finite closed systems, even though the average current that it predicts is correct for long times. This is because, in the case of elastic scattering, the current is dominated by local properties at the junction. On the other hand, other quantities of interest, such as the occupation of particles – whether at a quasi-steady state or not – are very sensitive to the full spatial extent of the wavefunctions.

The entanglement entropy from our simulations of the full quantum dynamics agrees with the formula derived from semi-classical FCS with a binomial distribution, which raises

the question of how the wave nature of the transmitted particles can be well approximated by such a distribution. We also found that quantum corrections are not significant in the equal-time number fluctuations of these noninteracting systems. On the one hand, this supports the use of a semi-classical approach in studying certain transport phenomena. On the other hand, finding transport coefficients that are sensitive to quantum corrections is an interesting future direction.

Extending those comparisons to higher dimensions or in the presence of interactions beyond mean field approximations could be very challenging, but they could lead to a deeper understanding of transport phenomena in closed quantum sys-

tems. We emphasize that these issues, such as the dynamics and feedback of reservoirs, quantum correlations, and matter-wave propagation, should be carefully investigated in more complex situations as we did here for non-interacting systems.

ACKNOWLEDGMENTS

C.C.C. acknowledges the support of the U.S. Department of Energy through the LANL/LDRD Program. MD acknowledges support from the DOE grant DE-FG02-05ER46204.

-
- [1] H. Ott, E. de Mirandes, F. Ferlaino, G. Roati, G. Modugno, and M. Inguscio, *Phys. Rev. Lett.* **92**, 160601 (2004).
 - [2] T. Salger, S. Kling, T. Hecking, C. Geckeler, L. Morales-Molina, and M. Weitz, *Science* **326**, 1241 (2009).
 - [3] U. Schneider, L. Hackermüller, J. P. Ronzheimer, S. Will, S. Braun, T. Best, I. Bloch, E. Demler, S. Mandt, D. Rasch, and A. Rosch, *Nat. Phys.* **8**, 213 (2012).
 - [4] R. A. Pepino, J. Cooper, D. Z. Anderson, and M. J. Holland, *Phys. Rev. Lett.* **103**, 140405 (2009).
 - [5] A. Ramanathan, K. C. Wright, S. R. Muniz, M. Zelan, W. T. Hill III, C. J. Lobb, K. Helmerson, W. D. Phillips, and G. K. Campbell, *Phys. Rev. Lett.* **106**, 130401 (2011).
 - [6] J. P. Brantut, J. Meineke, D. Stadler, S. Krinner, and T. Esslinger, *Science* **337**, 1069 (2012).
 - [7] J. G. Lee, B. J. Mcllvain, C. J. Lobb, and W. T. Hill, *Sci. Rep.* **3**, 1034 (2013).
 - [8] A. A. Zozulya and D. Z. Anderson, *Phys. Rev. A* **88**, 043641 (2013).
 - [9] S. Eckel, J. G. Lee, F. Jendrzejewski, N. Murray, C. W. Clark, C. J. Lobb, W. D. Phillips, M. Edwards, and G. K. Campbell, *Nature* **506**, 200 (2014).
 - [10] R. Landauer, *IBM J. Res. Dev.* **1**, 223 (1957).
 - [11] M. D. Ventra, *Electrical Transport in nanoscale systems* (Cambridge University Press, Cambridge, UK, 2008).
 - [12] G. M. Bruun and H. Smith, *Phys. Rev. A* **72**, 043605 (2005).
 - [13] T. Schafer and D. Teaney, *Rep. Prog. Phys.* **72**, 126001 (2009).
 - [14] J. P. Brantut, C. Grenier, J. Meineke, D. Stadler, S. Krinner, C. Kollath, T. Esslinger, and A. Georges, *Science* **342**, 713 (2013).
 - [15] M. Bruderer and W. Belzig, *Phys. Rev. A* **85**, 013623 (2012).
 - [16] D. B. Gutman, Y. Gefen, and A. D. Mirlin, *Phys. Rev. B* **85**, 125102 (2012).
 - [17] D. P. Simpson, D. M. Gangardt, I. V. Lerner, and P. Kruger, *Phys. Rev. Lett.* **112**, 100601 (2014).
 - [18] I. Klich and L. Levitov, *Phys. Rev. Lett.* **102**, 100502 (2009); *Advances in Theoretical Physics: Landau Memorial Conference*, Edited by V. Lebedev and M. V. Feigelman (AIP Conference Proceedings), volume 1134, 36-45 (2009).
 - [19] M. Di Ventra and T. Todorov, *J. Phys. Cond. Matt.* **16**, 8025 (2005).
 - [20] N. Bushong, N. Sai, and M. Di Ventra, *Nano Lett.* **5**, 2569 (2005).
 - [21] S. Kurth, G. Stefanucci, C. O. Almbladh, A. Rubio, and E. K. U. Gross, *Phys. Rev. B* **72**, 035308 (2005).
 - [22] C. L. Cheng, J. S. Evans, and T. V. Voorhis, *Phys. Rev. B* **74**, 155112 (2006).
 - [23] C. C. Chien, M. Zwolak, and M. Di Ventra, *Phys. Rev. A* **85**, 041601(R) (2012).
 - [24] C. C. Chien and M. Di Ventra, *EPL* **99**, 40003 (2012).
 - [25] C. C. Chien and M. Di Ventra, *Phys. Rev. A* **87**, 023609 (2013).
 - [26] C. C. Chien, D. Gruss, M. Di Ventra, and M. Zwolak, *New J. Phys.* **15**, 063026 (2013).
 - [27] G. W. Chern, C. C. Chien, and M. Di Ventra, *Eprint*, arXiv: 1307.6128.
 - [28] S. Peotta and M. Di Ventra, *Phys. Rev. A* **89**, 013621 (2014).
 - [29] K. Henderson, C. Ryu, C. MacCormic, and M. G. Boshier, *New J. Phys.* **11**, 043030 (2009).
 - [30] A. L. Gaunt, T. F. Schmidutz, I. Gotlibovych, R. P. Smith, and Z. Hadzibabic, *Phys. Rev. Lett.* **110**, 200406 (2013).
 - [31] L. Susskind and J. Lindesay, *The holographic universe: An introduction to black holes, information and the string theory revolution* (World Scientific, 2005).
 - [32] M. A. Nielsen and I. L. Chuang, *Quantum Computation and Quantum Information* (Cambridge University Press, 2001).
 - [33] H. F. Song, C. Flindt, S. Rachel, I. Klich, and K. Le Hur, *Phys. Rev. B* **83**, 161408(R) (2011).
 - [34] H. F. Song, S. Rachel, C. Flindt, I. Klich, N. Laflorencie, and K. Le Hur, *Phys. Rev. B* **85**, 035409 (2012).
 - [35] For example, no QSSC is found in a tilted lattice potential. Moreover, if the initial filling has certain patterns (one particle per few sites), there is also no QSSC, as one can infer from Sec. IV.
 - [36] M. Zwolak and M. Di Ventra, *App. Phys. Lett.* **81**, 925 (2002).
 - [37] For the weak-link case, one may pick either the last (first) site on the left (right) lattice. The current is not affected by the choice if $E_C = E_{L,R}$ is chosen accordingly.
 - [38] F. Heidrich-Meisner, S. R. Manmana, M. Rigol, A. Muramatsu, A. E. Feiguin, and E. Dagotto, *Phys. Rev. A* **80**, 041603 (2009).
 - [39] A. Polkovnikov, K. Sengupta, A. Silva, and M. Vengalattore, *Rev. Mod. Phys.* **83**, 863 (2011).
 - [40] M. Beria, Y. Iqbal, M. Di Ventra, and M. Muller, *Phys. Rev. A* **88**, 043611 (2013).
 - [41] B. T. Seaman, M. Kramer, D. Z. Anderson, and M. J. Holland, *Phys. Rev. A* **75**, 023615 (2007).
 - [42] T. Sabetta and G. Misguich, *Phys. Rev. B* **88**, 245114 (2013).
 - [43] T. Antal, Z. Racz, A. Rakos, and G. M. Schutz, *Phys. Rev. E* **59**, 4912 (1999).
 - [44] K. H. Thomas and C. Flindt, *Phys. Rev. B* **89**, 245420 (2014).
 - [45] For smaller initial bias, the distributions on the two sides still evolve dynamically and a quasi steady-state current is maintained for a certain period, but an inversion of the population on the two sides may not occur during that period.

- [46] M. Cheneau, P. Barnettler, D. Poletti, M. Endres, P. Schaub, T. Fukuhara, C. Gross, I. Bloch, C. Kollath, and S. Kuhr, *Nature* **481**, 484 (2012).
- [47] R. Geiger, T. Langen, I. Mazets, and J. Schmiedmayer, *New J. Phys.* **16**, 053034 (2014).
- [48] R. Kubo, M. Toda, and N. Hashitsume, *Statistical Physics II: Nonequilibrium Statistical Mechanics*, 2nd ed. (Springer-Verlag, Berlin, 2004).
- [49] A. L. Fetter and J. D. Walecka, *Quantum Theory of Many-Particle Systems* (Dover Publications, New York, 2003).
- [50] A. P. Jauho, N. S. Wingreen, and Y. Meir, *Phys. Rev. B* **50**, 5528 (1994).